Supplemental Methods

Cell culture

Skin fibroblasts from human controls and patients with *RRM1* variants were validated with Sanger sequencing and screened negative for mycoplasma contamination. Fibroblasts from patient 4 were not available. Cells were grown in glucose-rich DMEM supplemented with 10% FBS, essential aa, L-glutamine, and penicillin-streptomycin. To promote quiescence, cells were grown at confluence for 10 days in glucose-rich DMEM supplemented with 0.1% FBS, essential aa, L-glutamine, and penicillin-streptomycin.

Muscle histopathology

Muscle biopsies were obtained from quadriceps. Tissues were fixed in formalin, fixed in glutaraldehyde, or unfixed and immediately frozen in isopentane-liquid nitrogen. H&E staining was performed on 4 μm-thick paraffin-embedded biopsy sections. The individual SDH, COX-, and sequential SDH/COX histochemical reactions were performed on 10 μm-thick cryosectioned biopsy samples of probands 1a, 3, and 4.

mtDNA quantitation

Mitochondrial DNA copy number was assessed by real-time PCR using an ABI PRISM 7000 sequence detection system using TaqMan MGB primers. Multiplex quantitative PCR in muscle biopsies was performed for both mtDNA and nuclear DNA using 12S rRNA and RNase P probes. The relative proportion of mtDNA to nuclear DNA in probands was compared to controls tested at the same time.

Multiple mtDNA deletions

The presence of multiple mtDNA deletions in patient muscle was assessed by Southern blot analysis. DNA was digested with a restriction enzyme that linearizes human mtDNA (PvuII), electrophoresed through agarose gels, and hybridized to a probe detecting mtDNA (Gene Link GeneProber GL557, #40-2055-41). Long range PCR protocols to detect multiple mtDNA deletions were previously described (1).

Whole exome sequencing

Family 1: WES was obtained from blood using Agilent SureSelectXT Human All Exon V5+UTRs capture and Illumina HiSeq2500 sequencing technology and analyzed for the presence of pathogenic mutations using the NextGENe software from Softgenetics and a proprietary analytical pipeline by Molecular Pathology of Columbia University.

Proband 3: WES was performed as previously described (2). Briefly, exome capture was attained using the Agilent Sure Select Human All Exon V5 (50 Mb) capture kit and sequenced using the Illumina GAIIx platform in 75 base pair reads. Reads were aligned to the human reference genome (UCSC hg19). Called variants were restricted to exonic (coding) or splice-site variants with a minor allele frequency of 0.01 (1%) or less from 378 in-house controls and external variant databases (GnomAD, NHLBI ESP, 1000 Genomes). Given the positive family history, autosomal dominant (heterozygous) inheritance was prioritized. Rare variants of nuclear genes associated with known mtDNA maintenance disorders were first analyzed. Next, variants were filtered using Gene Ontology (GO)-Terms to prioritize genes encoding products involved in mitochondrial function, DNA replication, or maintenance. GO-Terms employed were the wild-card term ‘mitochond*’, ‘DNA repair’, ‘replication’, ‘transcription’, ‘nucleotide’, ‘purine’, ‘pyrimidine’, ‘exonuclease’, ‘polymerase’, ‘topoisomerase’, ‘ligase’, ‘helicase’ and ‘nucleoside’.

Copy number variants (CNVs) were also examined using the same GO-Terms. The identified *RRM1* variant was confirmed by Sanger sequencing.

Proband 4: Diagnostic WES was performed as described previously (3).

Magnetic resonance imaging

MRI of the brain of proband 1a without intravenous contrast was performed using multisequence multiplanar technique.

Structural analysis and molecular dynamics (MD) simulations

Structural analysis, tertiary alignments, and visualizations of hRRM1 (PDB: 3hne) and *S. cerevisiae* RNR1 (PDB: 1zyz) PDB structures were carried out using PyMOL Molecular Graphics System (Version 1.8 Schrödinger, LLC). Primary structure alignments were performed using MUSCLE (4).

For MD simulations of the RRM1 variants, we used the X-ray structure of the human RRM1-TTP-GDP complex in its dimeric form at 3.21Å resolution (PDB ID 3HND). The RRM1 dimer consists of chains A and B, with residues 14-742 and 2-742, respectively, including Mg^{2+}, GTP, TTP, and crystal water.

There are two cysteine residues, C352 and C356, close to the p.R381C variant. We modeled the C381-C356 disulfide bond for three reasons: (1) the sequence alignment between hRRM1 and ScRR1 in the Supplemental Figure 2A showed C352 (hRRM1) and S352 (ScRR1), and C356 (hRRM1) and A356 (ScRR1), and the hydrophobic property of Cys matched more closely with Ala than polar residue Ser; (2) both cysteine residues (C352 and C356) are in the loop region and have equal chances to form a disulfide bond with C381; and (3) in the WT there are hydrogen bonds between the guanidinium sidechain of R381 and the carboxyl group of E355, which makes R381 closer to neighboring C356.

The RRM1 was loaded into Maestro and processed using Schrödinger's Protein Preparation Wizard Panel (5) with default options such as missing hydrogen atoms and sidechain atoms and optimization of hydrogen bonding networks. Also, the optimal protonation states for histidine residues capped the N- and C- terminal ends with acetyl (ACE) and methyl amide (NMA) groups, respectively. Finally, the preprocessed structure was restraint minimized using an OPLS forcefield that minimizes hydrogen atoms while restraining the backbone and sidechain heavy atoms. The *3D Builder* panel in Maestro was used to mutate residue R381 to C381 and H381. The final structure was further solvated with explicit water and ions in the cubic box for further molecular dynamics (MD) simulations.

We used all-atom explicit solvent MD simulations to investigate the conformational changes of RRM1 variants. The CHARMM-GUI *solution builder* (6) was used to prepare the system for these simulations. RRM1 was solvated in a cubic box with a dimension of 144.0 x 144.0 x 144.0 $Å^3$. The system contained 0.15 M NaCl, and simulations were conducted at 310 K. The interactions between protein and water residues are modeled using CHARMM36 (7) force field and TIP3P (8) water. The forcefield parameters for TTP, GDP, and Mg^{2+} were obtained from CGenFF (9). All simulations were run using GPU-version of GROMACS v5.1.4 (10). The simulation protocol started with energy minimization of 1000 steps, followed by constant atoms, volume, and temperature (NVT) equilibration (1 fs per time step) and NPT (2 fs per time step) simulations for 5 ns before start of the production simulations. During the initial minimization and equilibration, the backbone, sidechain, and dihedral restraints were applied, and in the production, the run protein was allowed to move freely without any restraint. Temperature and pressure during the equilibration phase were maintained at 310 K and 1 bar, respectively, using Berendsen thermostat (11) and barostat. For the production run, a Nose-Hoover thermostat was used to control the temperature using a collision frequency of 1.0 ps^{-1}. Lennard-Jones and electrostatic interactions were calculated explicitly within a cutoff of 1.2 nm,

and long-range electrostatic interactions were calculated by particle mesh Ewald summation. The equilibration simulations were done on the NVT ensemble, and production run at constant atoms, pressure, and temperature (NPT) ensemble for 100ns. The total MD simulation time for all variants was 300 ns. The RRM1 WT, R381C, and R381H mutants contained ~281K atoms.

MD simulation trajectory analysis and visualization were done using Visual Molecular Dynamics (VMD 1.9.3) (12). Root mean square deviation (RMSD) was calculated using the RMSD trajectory tool in VMD. The distance between the center of mass (COM) of atoms was calculated using the VMD in-house Tcl scripts. The solvent-accessible surface area (SASA) and buried surface area (BSA) was calculated using the VMD measure *sasa* command with a probe of radius of 1.4 Å. All other time series figures were generated using Python scripts.

Ribonucleotide reductase activity

Measurement of RNR activity was assessed in actively cycling fibroblasts with a protocol adapted from Jong et al (13). Briefly, and to note protocol adaptations, fibroblasts were suspended 50 mM Tris pH 7.6, 20% glycerol, 15 mM $MgCl_2$, and 4 mM DTT and lysed by sonication. 500 μg protein was precipitated with 60% ammonium sulfate. Supernatant was passed through a G25 Sephadex column (Sigma, G25150). Reaction was performed at 25°C for 60 min with 3 nmol [2-^{14}C] CDP (Moravek, MC 480), 72 nmol cold CDP, 200 nmol ATP, 1.6 μM $MgCl_2$, 5 μM HEPES pH 7.6, 300 pmol thioredoxin, 10 nmol EDTA, 10 mM DTT, and 500 μg cell extract. Reaction product was run through 3.5 cm Dowex cation column, and fractions were read at A270 nm to detect separation of CMP and dCMP. [^{14}C] was measured from fractions to quantify RNR activity.

As an alternative measurement of RNR activity, fibroblasts were suspended in 50 mM Tris pH 7.6, 20% glycerol, 15 mM $MgCl_2$, and 4 mM DTT and lysed by passing through a 22G needle. After centrifugation, supernatant was passed through a G25 Sephadex column. RNR

activity was performed at 25°C for 60 min with 3 nmol [2-^{14}C] CDP, 350 μM CDP, 80 mM HEPES pH 7.6, 160 μM EDTA, 3.15 mM ATP, 20 mM DTT, 250 mM $MgCl_2$, 4.7 μM thioredoxin. This was followed by addition of 2.8 U NDP kinase and incubation at 25°C for 60 min. [2-^{14}C] CTP was measured using the DNA polymerase extension assay described by Martí, et al (14).

Nucleotide measurements

Ribonucleotides were extracted from fibroblast cultures (50-60% confluency) by acidic lysis. Cells grown in 100 mm plates were treated with 300 μL perchloric acid (final concentration 0.5 M) and centrifuged at 20,000 g for 5 min at 4°C. Supernatants were neutralized with 1.5 volumes 0.5 M tri-N-octylamine in Freon (1,1,2-trichlorotrifluoroethane) and centrifuged for 10 min at 10,000 g at 4°C. The aqueous phase was dried under speed vacuum and lyophilized extracts were resuspended in 100 μL of 20 mM ammonium acetate (pH 8.2). NTPs were resolved and determined with an Acquity UPLC-MS/MS apparatus (Acquity UPLC-Xevo™ TQ Mass Spectrometer; Waters, Milford, MA) using an Acquity UPLC BEH C18 column (100 x 2.1 mm, 130 Å pore, 1.7 μm particle; Waters) and an ion pairing-based elution using N,N-dimethylhexylamine (DMHA) as previously described (15).

To measure mitochondrial dNTP pools, actively cycling fibroblasts were collected and analyzed as previously described by Martí et al (14).

Alkaline hydrolysis and Southern blot

DNA isolated from fibroblasts was hydrolyzed with 0.3 M KOH for 4 h at 55°C. DNA was then run out on a denaturing gel (50 mM NaOH, 1 mM EDTA), followed by Southern blot detection of mtDNA (Gene Link GeneProber GL557, #40-2055-41).

Western blot

Antibodies used for western blots included RRM1 (Abcam, ab137114), α tubulin (Abcam, ab7291), and total OxPhos Human WB Antibody Cocktail (Abcam, ab110411).

Statistics

We used two-way ANOVA with one-subject per cell method to compare the mean outcome of each proband to the controls. The validity for such an approach relied on the plausible assumption that the group difference in mean of the outcomes of interest does not depend on experiment. Therefore, the model only included group and experiment as the main effect but no group by experiment interaction (as such an interaction cannot be determined from the study data even if it existed). Findings were considered as statistically significant if the corresponding p-values were less than 0.05. Statistical analysis was performed using SPSS Version 28.

Supplemental References

1. Blakely EL, Butterworth A, Hadden RD, Bodi I, He L, McFarland R, et al. MPV17 mutation causes neuropathy and leukoencephalopathy with multiple mtDNA deletions in muscle. *Neuromuscul Disord.* 2012;22(7):587-91.
2. Nicholls TJ, Nadalutti CA, Motori E, Sommerville EW, Gorman GS, Basu S, et al. Topoisomerase 3alpha Is Required for Decatenation and Segregation of Human mtDNA. *Mol Cell.* 2018;69(1):9-23 e6.
3. Wortmann SB, Koolen DA, Smeitink JA, van den Heuvel L, and Rodenburg RJ. Whole exome sequencing of suspected mitochondrial patients in clinical practice. *J Inherit Metab Dis.* 2015;38(3):437-43.
4. Edgar RC. MUSCLE: multiple sequence alignment with high accuracy and high throughput. *Nucleic Acids Res.* 2004;32(5):1792-7.
5. Sastry GM, Adzhigirey M, Day T, Annabhimoju R, and Sherman W. Protein and ligand preparation: parameters, protocols, and influence on virtual screening enrichments. *J Comput Aided Mol Des.* 2013;27(3):221-34.
6. Lee J, Cheng X, Swails JM, Yeom MS, Eastman PK, Lemkul JA, et al. CHARMM-GUI Input Generator for NAMD, GROMACS, AMBER, OpenMM, and CHARMM/OpenMM Simulations Using the CHARMM36 Additive Force Field. *J Chem Theory Comput.* 2016;12(1):405-13.
7. Klauda JB, Venable RM, Freites JA, O'Connor JW, Tobias DJ, Mondragon-Ramirez C, et al. Update of the CHARMM all-atom additive force field for lipids: validation on six lipid types. *J Phys Chem B.* 2010;114(23):7830-43.
8. Jorgensen WL, Chandrasekhar J, Madura JD, Impey RW, and Klein ML. Comparison of Simple Potential Functions for Simulating Liquid Water. *J Chem Phys.* 1983;79(2):926-35.

9. Vanommeslaeghe K, Hatcher E, Acharya C, Kundu S, Zhong S, Shim J, et al. CHARMM general force field: A force field for drug-like molecules compatible with the CHARMM all-atom additive biological force fields. *J Comput Chem.* 2010;31(4):671-90.

10. Pall S, Abraham MJ, Kutzner C, Hess B, and Lindahl E. Tackling Exascale Software Challenges in Molecular Dynamics Simulations with GROMACS. *Lect Notes Comput Sc.* 2015;8759:3-27.

11. Berendsen HJC, Postma JPM, Vangunsteren WF, Dinola A, and Haak JR. Molecular-Dynamics with Coupling to an External Bath. *J Chem Phys.* 1984;81(8):3684-90.

12. Humphrey W, Dalke A, and Schulten K. VMD: Visual molecular dynamics. *J Mol Graph Model.* 1996;14(1):33-8.

13. Jong AY, Yu KF, Zhou BS, Frgala T, Reynolds CP, and Yen Y. A simple and sensitive ribonucleotide reductase assay. *J Biomed Sci.* 1998;5(1):62-8.

14. Marti R, Dorado B, and Hirano M. Measurement of Mitochondrial dNTP Pools. *Mitochondrial Disorders: Biochemical and Molecular Analysis.* 2012;837:135-48.

15. Camara Y, Gonzalez-Vioque E, Scarpelli M, Torres-Torronteras J, Caballero A, Hirano M, et al. Administration of deoxyribonucleosides or inhibition of their catabolism as a pharmacological approach for mitochondrial DNA depletion syndrome. *Hum Mol Genet.* 2014;23(9):2459-67.

Supplemental Figure 1

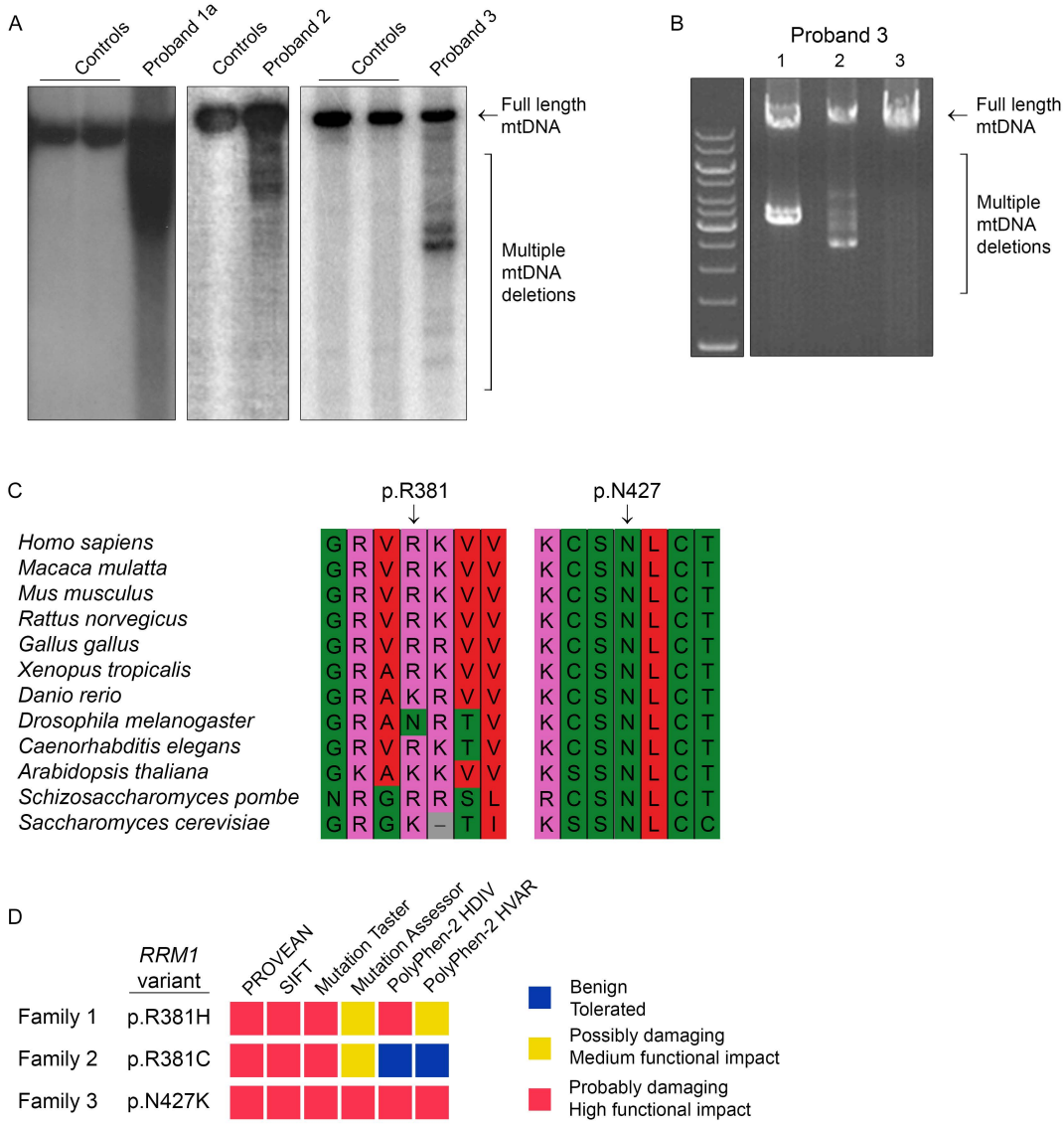

Supplemental Figure 1. Identification of MDDS and *RMM1* variants in probands. (A) Southern blots of mtDNA from control and proband muscle biopsies, where smears and small fragments indicate mtDNA multiple deletions. **(B)** Long-range PCR of muscle mtDNA comparing a proven case with a single mtDNA deletion (lane 1), proband 3 (lane 2), and an age-matched control (lane 3). **(C)** Multiple sequence alignment of RRM1 aa sequences with a Clustal X color scheme indicating residue type. **(D)** Predictions by software tools assessing the impact of *RRM1* variants on RRM1 protein integrity and function.

Supplemental Figure 2

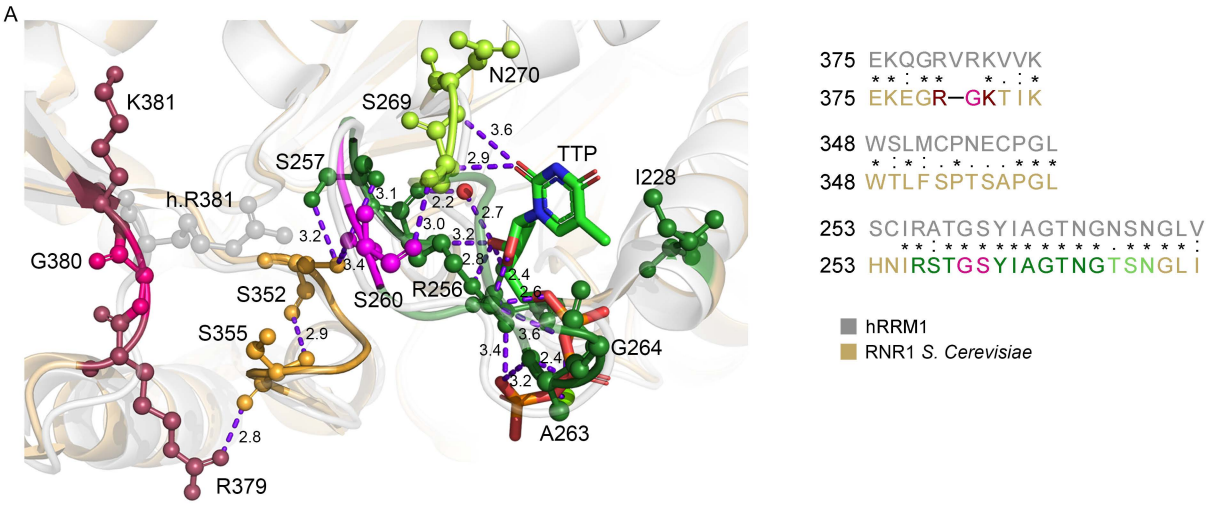

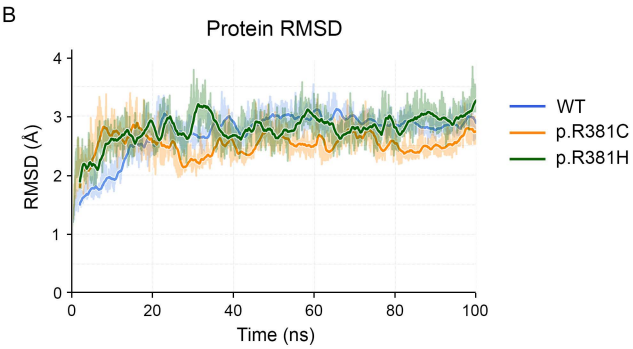

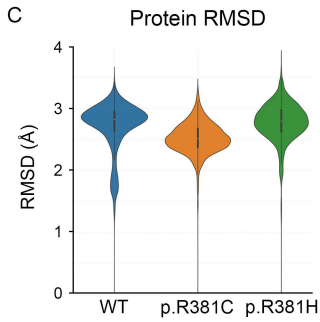

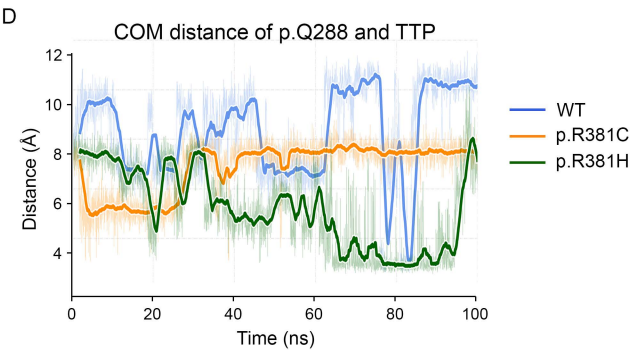

Supplemental Figure 2. Structural analysis of WT RRM1 and proband variants. (A) Structural alignment of human (hRRM1) and S. cerevisiae (RNR1), illustrating p.G380 (pink) in place of the human p.R381 in both secondary and tertiary alignments. **(B)** Time evolution of the RMSD of WT RRM1 and variants. **(C)** Violin plot of RMSD data showing the median and distribution. **(D)** COM distance between p.Q288 and TTP.

Supplemental Figure 3

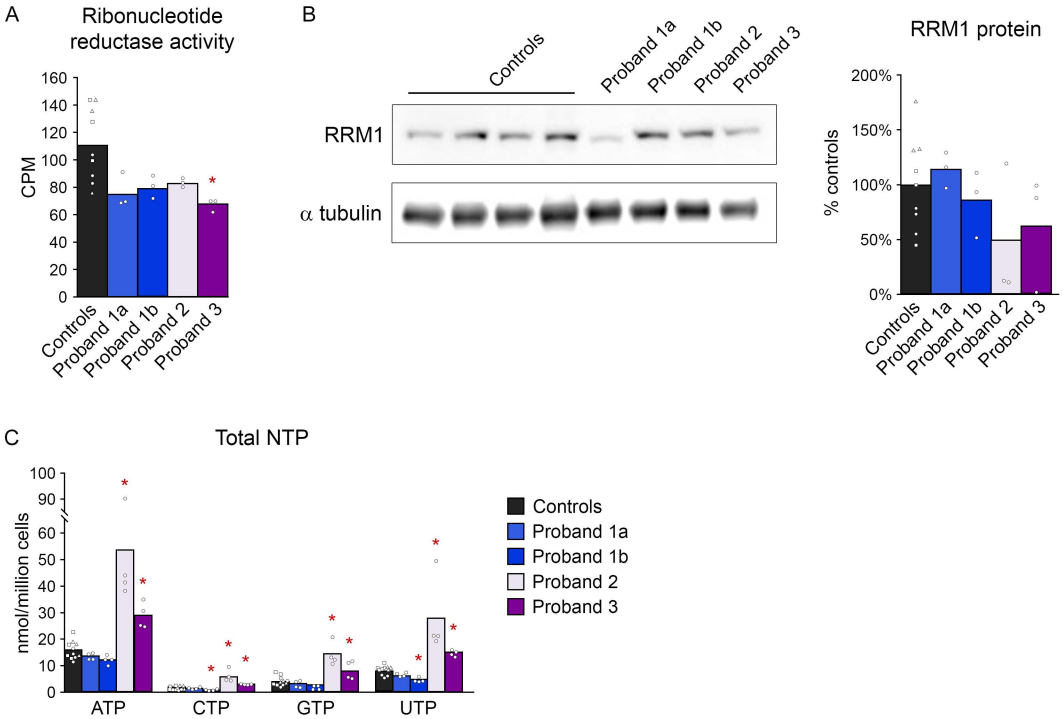

Supplemental Figure 3. RNR assessment of proband fibroblasts. (A) RNR activity of fibroblast protein extracts in the presence of excess ATP and [2-^{14}C] CDP, normalized by cell number input. **(B)** Representative western blot of RRM1 with α tubulin as a loading control. Bar graph depicts quantitation of 3 blots. **(C)** Total NTPs from proliferating fibroblasts quantitated from probands and 3 controls. *p<0.05.

Supplemental Figure 4

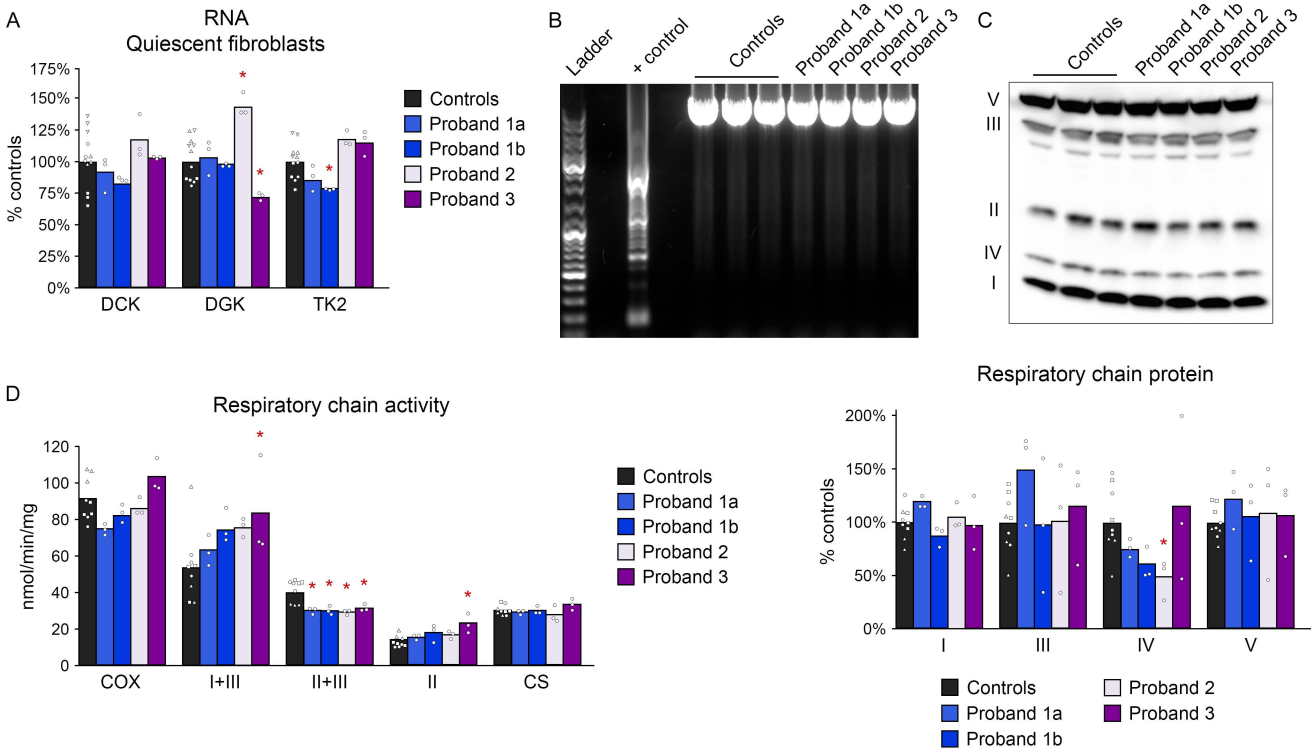

Supplemental Figure 4. Mitochondria and mtDNA in proband fibroblasts. (A) RNA was extracted from quiescent fibroblasts, quantitated by real-time RT-PCR, and normalized to GAPDH. **(B)** Long-range PCR of proliferating fibroblast DNA. **(C)** Representative western blot of proliferating fibroblasts with human OXPHOS antibody cocktail. Bar graph depicts quantitation of 3 blots. **(D)** Respiratory chain activity assay using fibroblast extracts from probands and 3 controls. *p<0.05.

Supplemental Figure 5

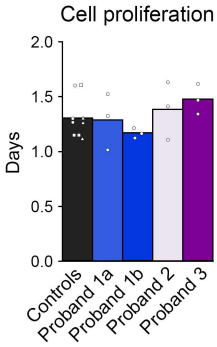

Supplemental Figure 5. Proliferation rate of proband fibroblasts. Fibroblasts were seeded at uniform densities and counted every 3 days. *p<0.05.